

RESEARCH

Open Access



VprBP regulates osteoclast differentiation via an epigenetic mechanism involving histone H2A phosphorylation

Yonghwan Shin¹, Sungmin Kim¹, Tae-Ik Choi², Cheol-Hee Kim² and Woojin An^{1*}

Abstract

Background Bone remodeling is a continuous and balanced process which relies on the dynamic equilibrium between osteoclastic bone resorption and osteoblastic bone formation. During osteoclast differentiation, pro-osteoclastogenic and anti-osteoclastogenic genes are selectively targeted by positive and negative transcription regulators, respectively. VprBP, also known as DCAF1, is a recently identified kinase and plays an important role in driving epigenetic gene silencing and oncogenic transformation. However, nothing is currently known about a possible involvement of VprBP in signaling pathways that regulate other cellular processes.

Results We demonstrate that VprBP stimulates RANKL-induced differentiation of osteoclast precursor cells (OCPs) into mature osteoclasts by suppressing the expression of anti-osteoclastogenic genes through phosphorylation of threonine 120 on histone H2A (H2AT120p). H2AT120p is critical for VprBP function, because abrogating VprBP kinase activity toward H2AT120 transcriptionally reactivates anti-osteoclastogenic genes and significantly attenuates osteoclast differentiation. Consistent with this notion, our in vivo studies established the importance of VprBP-mediated H2AT120p in low bone mass phenotypes and osteoporosis caused by overactive osteoclasts.

Conclusions Our data reveal a previously unrecognized function of VprBP in supporting RANKL-induced osteoclast differentiation and the molecular mechanism underlying its action as a negative regulator of anti-osteoclastogenic genes.

Keywords Histone, Chromatin, Epigenetic, VprBP, Phosphorylation, Osteoclast

Background

The HIV-1 Vpr Binding Protein (VprBP), also known as DDB1 and CUL4 Associated Factor 1 (DCAF1), is a large nuclear protein whose function has been explored with respect to its role in regulating cell cycle, cell growth, and

cell division [1–4]. Since VprBP interacts with CUL4-DDB1 ubiquitin ligase complex, it has been believed that such VprBP function is mainly achieved by directing polyubiquitination and proteasomal degradation of specific protein targets [1–3]. However, our recent study has uncovered that VprBP possesses an intrinsic kinase activity and phosphorylates histone H2A on threonine 120 (T120) in cancer cells [5–7]. In accordance with the idea that VprBP-mediated H2AT120 phosphorylation (H2AT120p) is an oncogenic signal, our gene expression profiling clearly indicated that silencing growth regulatory genes reflects the primary role of VprBP in cancer cells [5–7]. H2AT120p is critical for VprBP oncogenic potential, because VprBP kinase-dead mutation

*Correspondence:

Woojin An
woojinan@usc.edu

¹ Department of Biochemistry and Molecular Medicine, Norris Comprehensive Cancer Center, University of Southern California, Los Angeles, CA 90033, USA

² Department of Biology, Chungnam National University, Daejeon, Republic of Korea



© The Author(s) 2024. **Open Access** This article is licensed under a Creative Commons Attribution-NonCommercial-NoDerivatives 4.0 International License, which permits any non-commercial use, sharing, distribution and reproduction in any medium or format, as long as you give appropriate credit to the original author(s) and the source, provide a link to the Creative Commons licence, and indicate if you modified the licensed material. You do not have permission under this licence to share adapted material derived from this article or parts of it. The images or other third party material in this article are included in the article's Creative Commons licence, unless indicated otherwise in a credit line to the material. If material is not included in the article's Creative Commons licence and your intended use is not permitted by statutory regulation or exceeds the permitted use, you will need to obtain permission directly from the copyright holder. To view a copy of this licence, visit <http://creativecommons.org/licenses/by-nc-nd/4.0/>.

significantly impaired cancer cell proliferation and xenograft tumor growth [5–7]. Considering that VprBP-mediated H2AT120 plays a causal role in uncontrolled cell growth, we also have developed a small-molecule inhibitor, named B32B3, capable of inactivating VprBP kinase activity, attenuating H2AT120p, and blocking tumor growth in xenograft models [5–7]. Related, our additional investigation identified VprBP kinase activity targeting EZH2 (at T367) in colon cancer cells and p53 (at S367) in DNA damage-response cascade [8, 9], implying different mechanisms employed by VprBP in different types of cancer. While these observations highlight a direct link between VprBP kinase pathway and cancer development, a possible contribution of VprBP to other pathological events remains to be determined.

Bone remodeling is a dynamic process that involves the coordinated action of bone-forming osteoblasts and bone-resorbing osteoclasts [10, 11]. Osteoblasts are mesenchymal stem cells that form bone matrix, whereas osteoclasts are large multinucleated cells whose function is to resorb bone matrix [12–16]. Abnormal osteoclast generation and dysregulated bone degradation are responsible for many of malignant bone diseases, including osteoporosis, rheumatoid arthritis, Paget's disease, and tumor bone metastases [17]. During osteoclast differentiation, receptor activator of nuclear factor (NF)- κ B ligand (RANKL) is expressed as a membrane-anchored protein in osteoblasts and binds to its cognate receptor RANK on pre-osteoclast cell membrane [10, 18]. This receptor-bound RANKL together with macrophage-colony stimulating factor (M-CSF) initiates multiple signal transduction pathways to turn on osteoclastogenic transcription program and trigger the differentiation of osteoclast precursor (OCP) cells into mature osteoclasts [10, 18].

Taking into consideration that all osteoclastogenic genes are stored in the nucleus by chromatinization, it is highly likely that chromatin-dependent pathways account for fundamental mechanisms underlying osteoclast differentiation. This interesting possibility has not been investigated in great detail, but there is some evidence linking epigenetic chromatin reorganization to osteoclastogenic transcription program. For example, the expression of key osteoclastogenic genes is regulated by H3K4/H3K27 tri-methylation as well as H3 acetylation [19, 20]. Also, adding another pathway through which osteoclastogenesis is epigenetically controlled, our recent study identified a role for matrix metalloproteinase 9 (MMP-9) in clipping histone H3 N-terminal tails and conferring active expression properties to genes encoding pro-osteoclastogenic factors [21–23]. The observed role of MMP-9 has potential therapeutic implications since treatment with MMP-9 inhibitor can be used to

control aberrantly activated osteoclastogenic genes and thus osteoclast differentiation [21–23]. Hence, continuous identification and characterization of factors capable of triggering osteoclast differentiation are crucial for preventing and curing osteoporosis and other bone diseases.

In this study, we employed *in vitro* and *in vivo* model systems to investigate a possible role of VprBP as an epigenetic regulator of RANKL-induced osteoclast differentiation. Our data demonstrate that VprBP is highly expressed and catalyzes H2AT120p in response to RANKL stimulation, thereby suppressing a set of anti-osteoclastogenic genes and triggering OCP cells to differentiate into multinucleated mature osteoclasts. Consistent with these observations, inhibition and knockdown of VprBP impair H2AT120p, reactivate anti-osteoclastogenic genes, and reduce mature osteoclast formation. Our studies uncover a novel role for VprBP in RANKL-induced osteoclastogenesis and suggest that targeting VprBP kinase activity could be a promising therapeutic strategy to treat bone resorptive diseases.

Materials and methods

Antibodies

Antibodies used in this study are as follows: anti-Histone H2AT120p antibody from Active Motif; anti-EZH2T367p antibody from ABclonal Biocechnology; anti-VprBP and anti-EZH2 antibodies from Proteintech; and anti-Histone H2A antibody from Abcam.

Osteoclast differentiation and Western blotting

Osteoclast precursor (OCP) cells were prepared as recently described [21–23]. To generate osteoclasts, OCP cells were cultured in the presence of 30 ng/ml macrophage colony-stimulating factor (M-CSF) and 50 ng/ml receptor activator of nuclear factor kappaB ligand (RANKL). On days 0, 1, 3, and 5, the cells were fixed with formaldehyde and stained for tartrate-resistant acid phosphatase (TRAP) using an acid phosphatase leukocyte kit (Sigma). TRAP-positive multinucleated cells containing three or more nuclei were counted as osteoclasts under a light microscope. In certain instances, media were supplemented with DMSO or VprBP inhibitor B32B3 (0, 0.05, 0.1, 0.25, 0.5, and 1 μ M) to evaluate their effects on OCP cell differentiation. To determine the levels of H2AT120p, whole cell lysates were prepared from OCP-induced cells using M-PERTM Mammalian Protein Extraction Reagent (Thermo Fisher Scientific) according to the manufacturer's instructions. Total histone proteins were acid-extracted from the cultured cells and Western blot assays with prepared samples were conducted as described previously [5–9].

Cell viability assay

OCP-induced cells were cultured in 96-well plates at a density of 0.5×10^4 in the absence or presence of VprBP inhibitor B32B3 for 5 days. Cell viability was assessed by using the MTT (3-(4,5-dimethylthiazol-2-yl)-2,5-diphenyl-tetrazolium bromide) cell growth assay kit (Sigma) as detailed previously [7, 23, 24].

RNA interference and inhibitor treatment

DNA oligonucleotides (5'-ATGGCCAGCTCAGCTATATT-3') encoding shRNA specific for VprBP coding region were annealed and ligated into the lentiviral expression vector pLKO.1 (Addgene, Berkeley). Lentiviral particles were generated in 293 T cells by transfecting plasmids encoding VSV-G, NL-BH, and the shRNA. OCP cells were transduced with these viruses for 3 days prior to differentiation [21–23]. VprBP inhibitor B32B3 (0.5 μ M) was also used in differentiation assays together with RANKL in order to control VprBP kinase activity during RANKL-induced osteoclastogenesis.

RT-qPCR

Total RNA was isolated from OCP-induced cells by using the RNeasy Mini kit (Qiagen Inc.) and converted to first-strand cDNA using the SuperScript III First-Strand System Kit (Thermo Fisher Scientific). Real-time RT-qPCR was performed with SYBR Green Real-time PCR Master Mixes (Thermo Fisher Scientific) according to the manufacturer's instructions. The primers used for RT-qPCR are listed in Supplementary Table 1. All mRNA values were normalized to GAPDH mRNA levels, and all reactions were run in triplicate.

ChIP-qPCR

ChIP assays with OCP-induced cells were performed using the ChIP Assay Kit (Millipore) as recently described [8, 36]. After reversing protein–DNA crosslinks, immunoprecipitated DNA was purified and analyzed by qPCR using the primers that amplify the promoter (P), transcription start site (TSS), and coding region (C) of VprBP target genes. The primers used for qPCR are listed in Supplementary Table 2. Specificity of amplification was determined by melting curve analysis, and all samples were run in triplicate.

RNA-seq

RNA was extracted from OCP-induced cells using the Qiagen RNeasy kit (Qiagen Inc.) according to the manufacturer's instructions. RNA quality was assessed using an Agilent Bioanalyzer with the DNA1000 kit. Strand-specific libraries were generated from the isolated RNA using the KAPA Stranded mRNA-Seq Kit

with KAPA mRNA Capture Beads (Kapa Biosystems Inc.). The resulting libraries were pooled, denatured, and diluted to 15 pM before clonal clustering onto the sequencing flow cell using the Illumina cBOT Cluster Generation Station and Cluster Kit v3-cBot-HS. The clustered flow cell was sequenced using 1×50 SE reads on the Illumina HiSeq according to the manufacturer's protocol. Base conversion was performed using OLB version 1.9, and the resulting sequences were demultiplexed and converted to Fastq using CASAVA version 1.8 (Illumina) [7, 21, 24, 25]. The sequenced RNA-seq reads were then aligned to the mm10 GENCODE version 29 using STAR 2.6.1d (National Human Genome Research Institute (NHGRI)) [26, 27]. The aligned reads were quantified at the gene level, and gene counts were normalized using the upper quartile normalization method. Principal component analysis with normalized gene counts was performed, and differentially expressed genes were selected using the Gene Specific Algorithm from Partek Flow software, <https://www.partek.com/partek-flow/> (Partek Inc.). A volcano plot was generated using fold change and false discovery rate of genes, with a false discovery rate cutoff of 0.05 and absolute fold change > 2.5 to statistically detect significantly differentially expressed genes. Gene ontology analysis of differentially expressed genes was performed using the Ingenuity Pathway Analysis tool (IPA version 52,912,811) (Qiagen Inc.). Heatmaps were generated by calculating the Z score of gene expression levels using the Generalized Minimum Distance R package heatmap.3 function [28].

VprBP inhibitor treatment in zebrafish and calcein labeling

Zebrafish (*Danio rerio*) of the AB strain were maintained and raised under standard conditions in a circulating water system at 28 °C with day–night (14 h light/10 h dark) cycles according to the established protocols [29–31]. The fish were fed live brine shrimp three times a day. Male and female zebrafish with high potential to produce fertilized eggs were used for natural spawning. After removing unfertilized eggs, embryos were kept at 28 °C with day–night (14 h light/10 h dark) cycles. The zebrafish larvae were collected and maintained in petri dishes filled with E3 water (5.0 mM NaCl, 0.17 mM KCl, 0.33 mM CaCl₂, and 0.33 mM MgSO₄). At 6 dpf, the larvae were treated with 25 μ M PDS in the absence or presence of three different concentrations (0.3, 0.8, and 2 μ M) of the VprBP inhibitor B32B3 for 3 days. For calcein staining, a fluorescent dye staining method commonly used for detecting calcium as an indicator of mineralization [29, 32], zebrafish larvae were collected at 9 dpf (days post-fertilization) and immersed in a 1% working solution of calcein, C0875, (Sigma) for a duration of

10 min. Subsequently, the embryos were washed three times with E3 water (each wash lasting 3 min) to remove any unbound dye. The fluorescent signals of the calcein-stained vertebral column in the spinal region of the zebrafish were analyzed at 10× magnification using fluorescence microscopy equipped with a long-pass green filter (excitation 480±40 nm; emission 510 nm). All zebrafish studies were approved by the Institutional Animal Care and Use Committee and conducted in accordance with the guidelines set forth by the committee.

VprBP inhibitor treatment in mice

Seven-week-old male C57BL/6 mice were obtained from Charles River Laboratories (Wilmington, MA, USA). Mice were acclimatized under a constant light/dark cycle at 22±2 °C (12 h light / dark cycles) and served with a general laboratory diet and water ad libitum. Mice were injected with RANKL alone or RANKL and B32B3 together over the calvaria every other day, being alternatively treated with RANKL on the intervening days, for a total duration of 14 days. Six mice were injected for each group. 14 days after injections, mice were sacrificed, and calvaria was collected and fixed with 4% paraformaldehyde. Paraffin-embedded Sects. (6 µm) of calvaria were stained for hematoxylin/eosin and TRAP for histological analysis. Images were acquired with an Aperio ScanScope Model T3 and were analyzed with ImageScope software (Aperio Technologies) as described previously [33, 34]. All animal studies were conducted according to protocols approved by the Institutional Animal Care and Use Committee.

Micro-CT analysis

Calvarial bones were aseptically excised from euthanized mice and fixed in 4% paraformaldehyde as previously described [33, 34]. The micro-CT scanning was performed using a SkyScan 1172 scanner (Bruker, Belgium) with settings at 67 kV and 147 µA for 705 ms. Analysis of bone volume (mm³) relative to tissue volume and bone mineral density within the region of interest was conducted using 2D/3D Image analysis CT-analyzer software (Amira and Scanco). The regions of interest were

defined as the areas encompassing the coronal and sagittal sutures in the calvaria. For visualization purposes, the segmented data were imported and reconstructed into a three-dimensional image displayed using Vgstudio Max 3.3.2.

Statistical analysis

All quantitative data are presented as mean±standard deviation (SD). Statistical analyses of datasets were performed with Student's two-tailed t-test or two-way ANOVA followed by Bonferroni post-hoc test using GraphPad Prism software (GraphPad Software Inc.) which was used for all analyses of the experiments. A P value <0.05 was considered statistically significant.

Results

VprBP is a potent osteoclastogenic factor

In view of our published data demonstrating that epigenetic signaling pathways are critical for osteoclastogenesis [21–23, 33, 34], it was an interesting issue whether VprBP is also involved in this differentiation process. This study was initiated by the initial discovery that RANKL-induced differentiation of primary osteoclast precursor (OCP) cells to large multinuclear osteoclasts triggered a remarkable increase of VprBP mRNA and protein levels from day 3 after induction (Fig. 1A; Supplementary Fig. S1). In parallel experiments in which changes in H2AT120p were analyzed over the same time period, H2AT120p was also detectable in OCP cells cultured with RANKL for 3 and 5 days (Fig. 1A). The strong correlation between VprBP expression and H2AT120p led us to speculate that VprBP is the kinase responsible for catalyzing H2AT120p during osteoclastogenesis. In good agreement with this idea, specific knockdown of VprBP almost completely abrogated H2AT120p in OCP-induced cells (Fig. 1B). Since VprBP depletion also decreased the average number of mature osteoclasts in our differentiation assays (Fig. 1B), these results confirm the functional contribution of VprBP to RANKL-induced osteoclast formation.

In a previous study [5], we screened a large compound library and identified B32B3 as an inhibitor which

(See figure on next page.)

Fig. 1 VprBP kinase activity required for RANKL-induced osteoclastogenesis. **A, B** Primary OCP cells were treated with RANKL for 0, 1, 3, or 5 days, fixed with formaldehyde, stained for TRAP (tartrate-resistant acid phosphatase), and photographed under a light microscope (10×) (left panel). TRAP-positive cells containing three or more nuclei were counted as osteoclasts on the indicated days (middle panel). Whole cell lysate and chromatin fractions were also extracted from OCP-induced cells and analyzed by Western blotting with VprBP, H2AT120p, and H2A antibodies to assess VprBP-mediated H2AT120p (right panel). (scale bar, 100 µm). Shown are the representative results of three independent experiments. **C, D** OCP-induced cells were cultured in the presence of DMSO (C) or VprBP inhibitor B32B3 (D) for 0, 1, 3, and 5 days, and TRAP-stained (left panel) and counted (middle panel) as in (A and B). Whole cell lysate and chromatin fractions were also prepared and analyzed by Western blotting with VprBP, H2AT120p, and H2A antibodies to assess VprBP-mediated H2AT120p (right panel). Shown are the representative results of three independent experiments

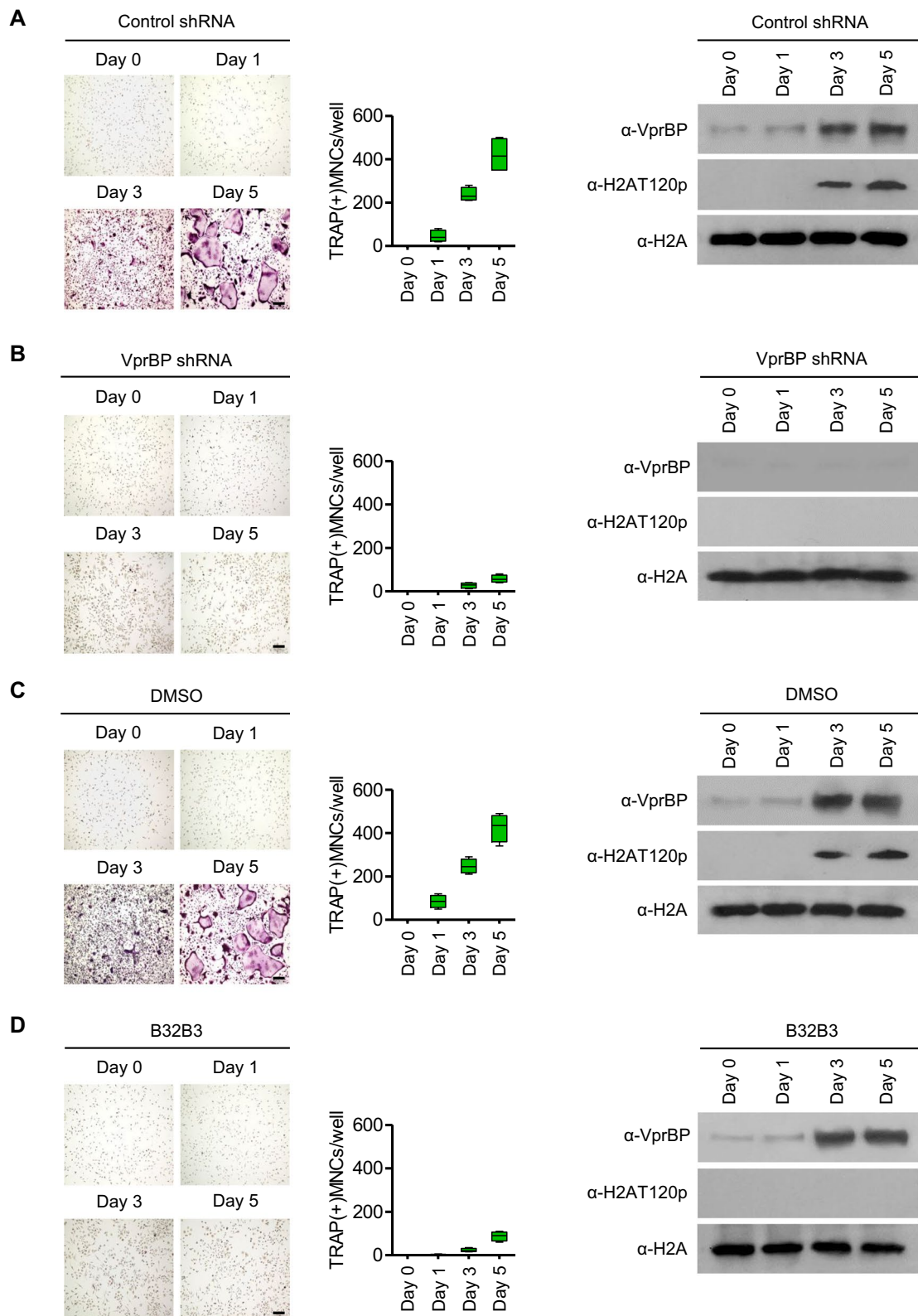


Fig. 1 (See legend on previous page.)

can selectively bind VprBP catalytic domain and block VprBP kinase activity. Given the demonstrated reliance of H2AT120p on VprBP in OCP-induced cells (Fig. 1B), we also sought to assess whether B32B3 treatment would recapitulate the effects of VprBP knockdown. When OCP-induced cells were exposed to six different concentrations (0, 0.05, 0.1, 0.25, 0.5, and 1 μ M) of B32B3, B32B3 was able to completely block H2AT120p at a concentration of 0.5 μ M without affecting cell viability (Supplementary Fig. S2A, B). Additionally, treating OCP-induced cells with 0.5 μ M B32B3 potently attenuated osteoclast differentiation in similar level as that observed with stable knockdown of VprBP (Fig. 1C, D; Supplementary Fig. S2C). These data point to the dependence of pro-osteoclastogenic function of VprBP on its kinase activity and underscore the notion that VprBP-dependent H2AT120p is critical for efficient osteoclastogenesis.

Related to the above observations, we recently showed that VprBP phosphorylates EZH2 at T367 (EZH2T367p) to augment its nuclear stabilization and enzymatic activity in colon cancer cells [8]. Thus, one would expect that VprBP also targets EZH2 for its osteoclastogenic function. However, consistent with previous reports [35, 36], we found that EZH2 is expressed mainly on day 1 of RANKL induction, whereas VprBP expression was observed 3 days following RANKL exposure (Supplementary Fig. S1). Also, knockdown of VprBP and treatment with B32B3 failed to generate any detectable changes in the levels of EZH2T367p in early phase of OCP-induced cell differentiation (Supplementary Fig. S1, S3). We thus speculate that the role of VprBP-mediated H2AT120p in OCP-induced cells is distinct from that of VprBP-mediated EZH2T367p in colon cancer cells. Such stage-specific functions of VprBP and EZH2 would predict that there might be additional activities and mechanisms to regulate their distinct contributions to RANKL-induced osteoclast differentiation.

VprBP suppresses anti-osteoclastogenic gene expression

As VprBP can repress gene transcription through H2AT120p in cancer cells [5–7], we next wanted to examine whether VprBP-mediated H2AT120p described above plays any role in regulating the transcription of certain genes during RANKL-induced osteoclast differentiation. Toward this end, we performed RNA sequencing (RNA-seq) with total RNA isolated from control and VprBP-depleted OCP-induced cells. In the principal component analysis of RNA-seq data, samples for each group were found to be markedly separated from each other, but close clustering of replicates from groups indicated minimal variability in the quality of analyzed replicates (Fig. 2A). Figure 2B, C, and Supplementary Fig. S4 depict the results of our comparative transcriptome

analysis with a fold change cutoff of 2.5, revealing that a total of 2202 genes were differentially expressed upon stable depletion of VprBP in OCP-induced cells. In more detailed examination, we found that 62% (1266) of those genes were activated in response to VprBP knockdown. Gene ontology analysis of 1266 downregulated targets also identified osteoarthritis pathway as the most up-regulated biological pathway in VprBP-depleted OCP-induced cells (Fig. 2D). Further supporting the role for VprBP in osteoclastogenesis, our analysis of the leading-edge subset in the gene set detected 18 genes encoding negative regulators of cell proliferation and differentiation (Fig. 2E). To validate the RNA-seq data, we next performed RT-qPCR on the 10 genes whose expression was activated upon VprBP depletion and which encode factors regulating cell proliferation and differentiation. As summarized in Fig. 3A, our analysis demonstrated that knockdown of VprBP led to a significant increase in the expression of the selected target genes in OCP-induced cells, clearly indicating the essential role for VprBP in suppressing target gene transcription. If OCP-induced cells were treated with VprBP inhibitor B32B3, the active state of target genes was also detected (Fig. 3C), again underscoring the importance of VprBP kinase activity for target gene silencing.

In an effort to investigate whether the observed function of VprBP reflects its direct effects on target genes, we next checked the levels of VprBP and H2AT120p at target genes by chromatin immunoprecipitation (ChIP) assays. Crosslinked chromatin was isolated from control and VprBP-depleted OCP-induced cells, and the precipitated DNA was amplified by quantitative real-time PCR (qPCR) using primer sets specific for promoters, transcription start sites, and coding regions of three representative VprBP-responsive genes, IRF8, MAFB, and TMEM119. Although the precipitation efficiency was slightly different among the target genes, we were able to detect much higher levels of VprBP ChIP-signals at the promoter region than at transcription start site and coding region in mock-depleted control OCP-induced cells (Fig. 3B), suggesting that VprBP targets the process of initiating transcription for its repressive action. Under these assay conditions, VprBP distribution patterns across the target genes were well correlated with H2AT120p enrichment patterns, indicating the direct involvement of VprBP in H2AT120p process. It was also apparent in our parallel ChIP-qPCR assays that VprBP occupancy of the target genes were significantly reduced after VprBP knock-down, and such changes also diminished the levels of H2AT120p, confirming a major role for VprBP in mediating H2AT120p at target genes (Fig. 3B). These observations were further corroborated by additional ChIP experiments in which exposure of OCP-induced

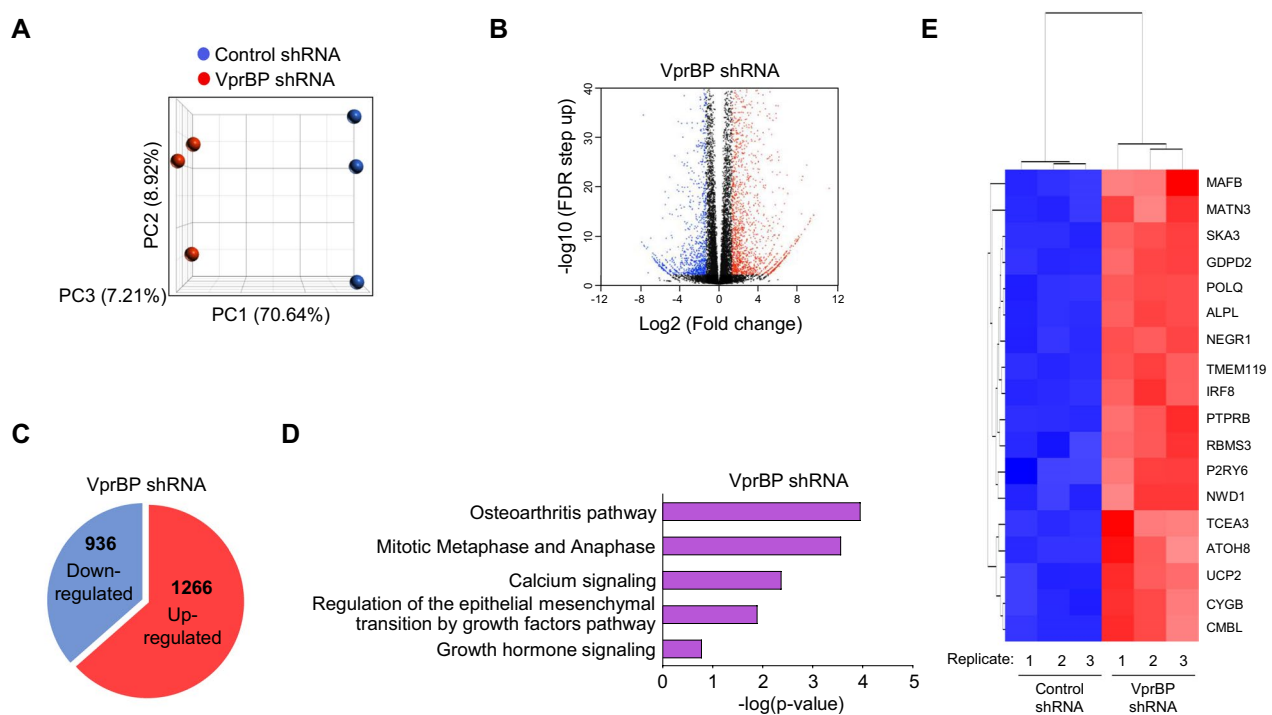


Fig. 2 Anti-osteoclastogenic genes inactivated by VprBP. **A** Principal component analysis (PCA) results of RNA-seq datasets generated in OCP-induced cells expressing a control shRNA or VprBP shRNA. VprBP knockdown (VprBP shRNA) group is shown in red, and control (control shRNA) group is shown in blue. Three replicates are generated per group. **B** A volcano plot of RNA-seq datasets is shown. $-\log_{10}(\text{FDR step up})$ is shown on the Y-axis, and fold change of gene expression between VprBP knockdown and control groups is shown on the X-axis. Genes modulated after VprBP depletion are colored in blue (downregulated) and red (upregulated). Three replicates are generated per group. **C** Venn diagram showing genes that are upregulated or downregulated (> 2.5 fold; $\text{FDR} < 0.05$) in VprBP-depleted OCP-induced cells compared to control OCP-induced cells. **D** Gene ontology analysis of the activated genes after knockdown of VprBP using Ingenuity Pathway Analysis (IPA version 52,912,811) tool developed by Qiagen. **E** Heatmap of 18 genes encoding cell proliferation and differentiation regulators significantly activated upon VprBP depletion. Normalized gene expression levels (Z-scores) are plotted. High and low expressions are shown in red and blue, respectively. Three replicates are generated per group

cells to VprBP inhibitor B32B3 still allowed VprBP occupancy but almost completely crippled H2AT120p at target genes (Fig. 3D). We thus concluded that VprBP-mediated H2AT120p is directly linked to the process of driving the inactivation of target genes in the process of RANKL-induced osteoclast differentiation.

VprBP modulates skeletal development and architecture in zebrafish and mouse models

The above-described effects of B32B3 strongly support the view that VprBP contributes to RANKL-induced osteoclastogenesis dependently of H2AT120p at anti-osteoclastogenic genes. If this is the case, then we can predict that B32B3 treatment is efficient in establishing the active state of bone development by impairing osteoclast differentiation and thus bone resorption. To explore this possibility, we decided to use zebrafish because it is an ideal model for the *in vivo* characterization of glucocorticoid-like drug-induced osteoporosis by treating larvae with prednisolone (PDS) [37, 38]. Expectedly, when

zebrafish larvae at 6 days post-fertilization (dpf) were treated with 25 μM PDS for 3 days and stained with 1% calcein, a significant enhancement of bone resorption was observed in this model system (Fig. 4A, B). However, the bone development defect arising from PDS treatment gradually disappeared in zebrafish co-treated with B32B3 over the concentration range of 0.3–2 μM (Fig. 4A, B), suggestive of the dominant effects of B32B3 over PDS and pointing to VprBP kinase activity as a key determinant of bone development. Considering that VprBP-mediated H2AT120p establishes the inactive state of anti-osteoclastogenic genes, it was also reasonable to speculate that B32B3 treatment should drive transcriptional reactivation of those target genes in PDS-exposed zebrafish. In good agreement with this idea, our RT-qPCR analysis detected a full recovery of target gene mRNA levels after co-treating PDS-exposed zebrafish with 2 μM B32B3 (Fig. 4C).

To further explore the significance of VprBP-mediated H2AT120p *in vivo*, we injected RANKL alone or

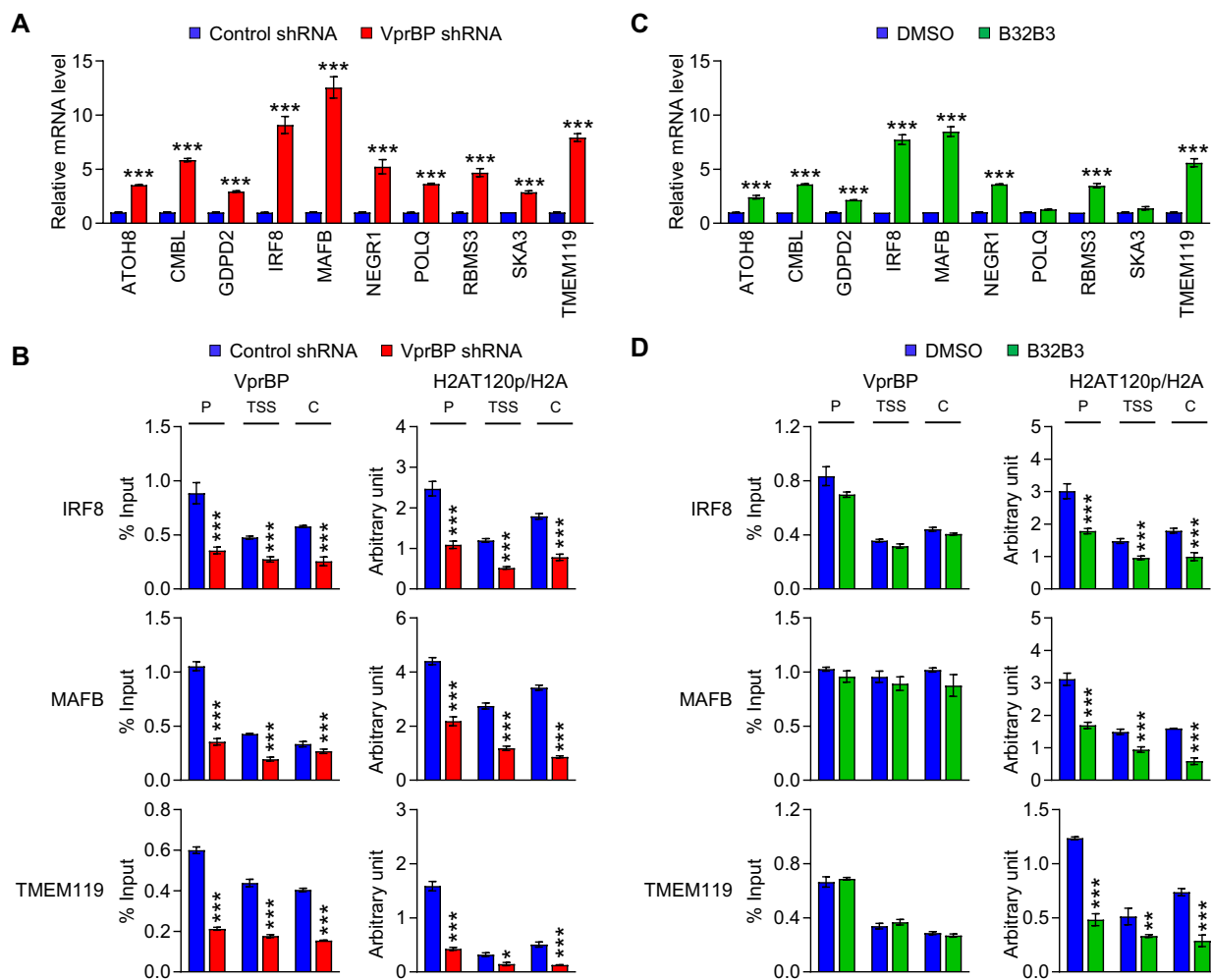


Fig. 3 VprBP transcription linked to H2AT120p at target gene promoters. **A** RNA samples were prepared from mock-depleted control and VprBP-depleted OCP-induced cells and analyzed by RT-qPCR using primers listed in Supplementary Table 1. All transcription levels were normalized to that of GAPDH. Data represents the mean \pm SD of three independent experiments. *** $P < 0.001$ versus control sh. **B** ChIP assays were performed in mock-depleted control and VprBP-depleted OCP-induced cells with VprBP, H2AT120p, and H2A antibodies as indicated. All ChIP DNAs were analyzed by real-time PCR with primer pairs amplifying the promoters (P), transcription start sites (TSS), and coding regions (C) of IRF8, MAFB, TMEM119 genes. Primers used are listed in Supplementary Table 2. Data were expressed as mean \pm SD ($N = 3$); * $p < 0.05$ and *** $p < 0.001$ versus control sh. **C** OCP-induced cells were treated with VprBP inhibitor B32B3, and VprBP target gene expression was analyzed by RT-qPCR as in (A). Data represents the mean \pm SD of three independent experiments. *** $P < 0.001$ versus DMSO. **D** ChIP assays were performed as in (B) but using B32B3-treated OCP-induced cells. Data were expressed as mean \pm SD ($N = 3$); ** $p < 0.01$ and *** $p < 0.001$ versus DMSO

RANKL plus B32B3 into the periosteal regions of male mouse calvaria every other day for 2 weeks. When we first tried increasing concentration of B32B3, RANKL-induced calvarial bone defect almost completely disappeared in mice treated with B32B3 at doses greater than 5 mg/kg (Supplementary Fig. S5). As seen in Fig. 5A, micro-computed tomography (micro-CT) analysis also indicated that B32B3 treatment promotes bone repair and regeneration at both periphery and center of RANKL-induced bone defects. These results were further supported by higher bone mineral density (BMD)

in mice treated with RANKL plus B32B3 compared to RANKL alone-treated mice (Fig. 5B). In accordance with these observations, we could confirm that co-treating mice with 5 mg/kg B32B3 under RANKL-treated conditions generated an apparent increase in the bone volume/tissue volume ratio (BV/TV) (Fig. 5B). Moreover, that mice treated with RANKL plus B32B3 display much smaller calvarial cavities in comparison with RANKL alone-treated counterparts argues persuasively that B32B3 prevents bone resorption, thereby ameliorating bone destruction (Fig. 5C). Again, the

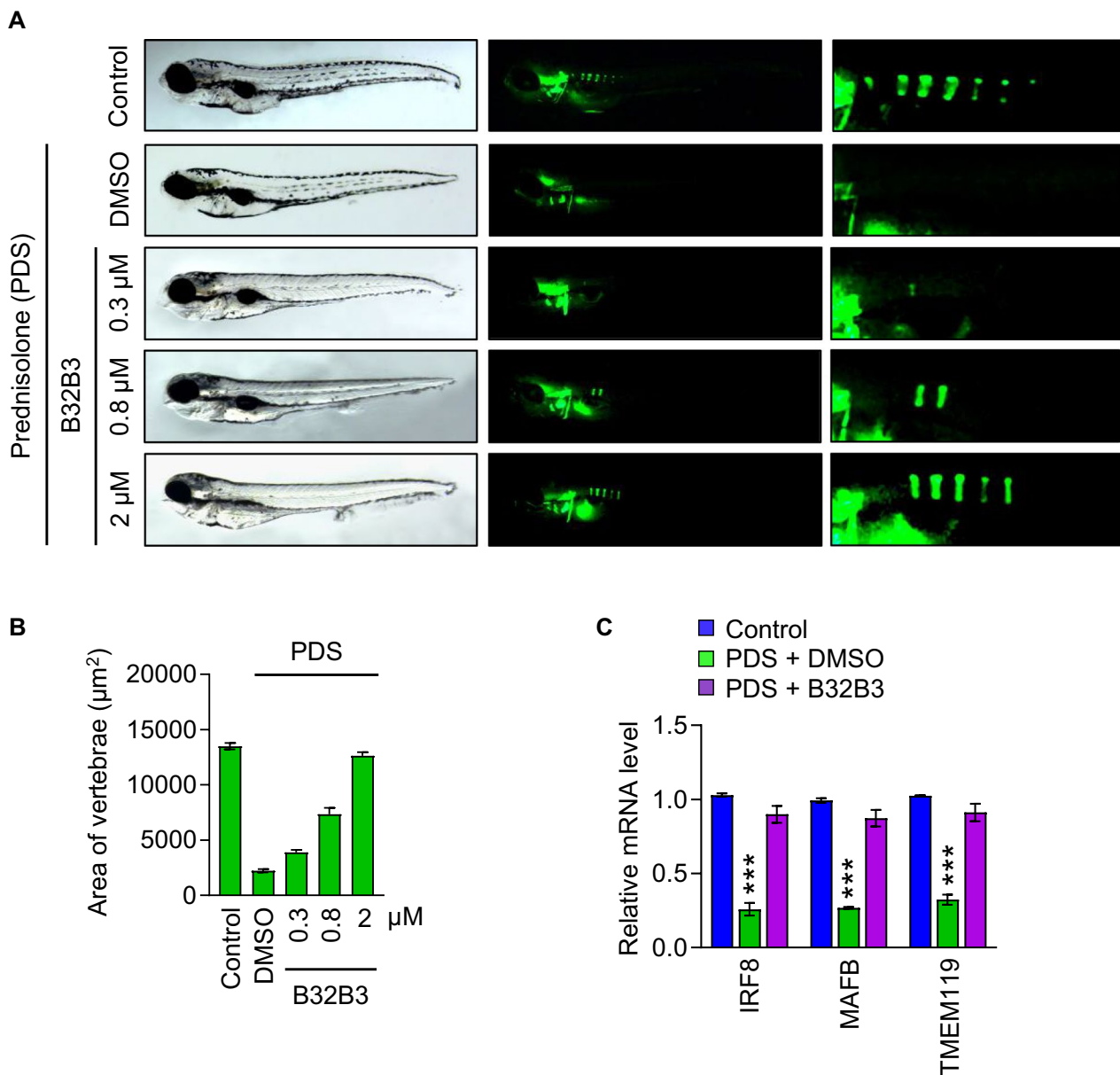


Fig. 4 Defective bone development in PDS-treated zebrafish rescued by VprBP inhibition. **A** Zebrafish larvae were treated with the indicated concentration of VprBP inhibitor B32B3 in the presence or absence of 25 μM prednisolone from 6 days post fertilization (dpf) to 9 dpf and stained with calcein to analyze skeletal mineralization. (*n* = 12 biologically independent experiment). **B** Zebrafish were treated as in (A) and relative bone mineral density was calculated by measuring the areas of the first five stained vertebrae. **C** Total RNA was extracted from PDS/B32B3-treated 9 dpf zebrafish larvae, and the expression levels of IRF8, MAFB, TMEM119 genes were quantified by RT-qPCR. Data represent the mean ± S.D of independent triplicate experiments. ****p* < 0.001 versus control

changes observed in response to B32B3 treatment were due to its impact on VprBP function as an epigenetic regulator of target gene transcription, because higher levels of anti-osteoclastogenic gene transcription were observed in mice treated with RANKL plus

B32B3 compared to RANKL alone-treated mice in our RT-qPCR analysis (Fig. 5D). These results reinforce our conclusion that B32B3-induced blockage of VprBP-mediated H2AT120p has negative impact on bone resorption and stimulates skeletogenesis by reactivating a group of anti-osteoclastogenic genes.

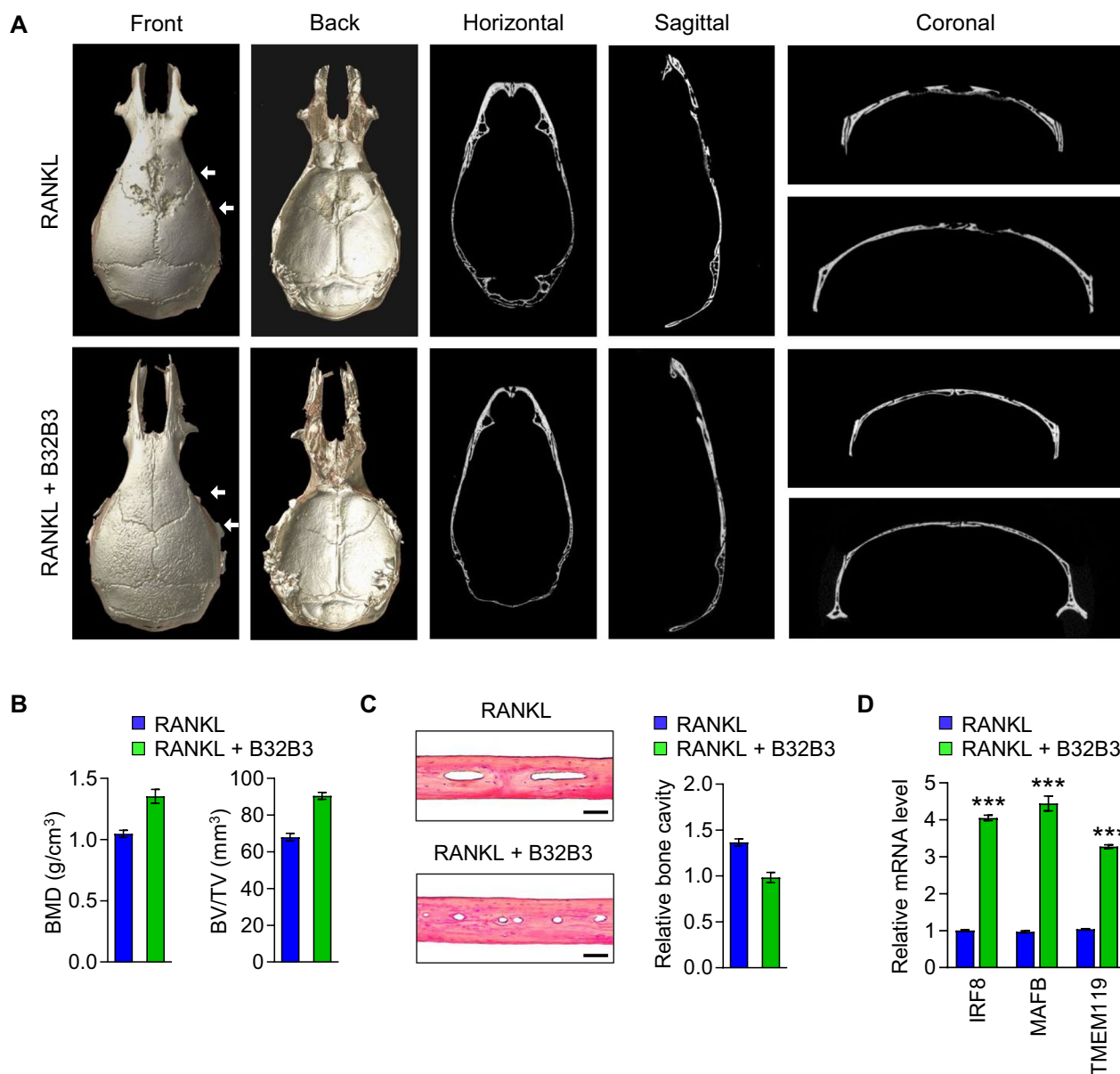


Fig. 5 RANKL-induced bone resorption in mice prevented by VprBP inhibition. **A** Seven-week-old male C57BL/6 mice were treated with RANKL alone (RANKL) or RANKL together with B32B3 (5 mg/kg) (RANKL+B32B3) every other day for 14 days. Mice were then sacrificed, and calvarial bones were subjected to micro-computed tomography (micro-CT) analysis. Three-dimensional micro-CT images representing various perspectives, including frontal, posterior, horizontal, sagittal, and coronal views, were acquired and are presented as representative illustrations in this study. (n=6 biologically independent experiment). **B** Bone mineral density (BMD) (left panel) and bone volume (BV) (right panel) per tissue volume were quantified using three-dimensional micro-computed tomography (micro-CT) images. **C** Bone sections were prepared from C57BL/6 mice treated with RANKL and B32B3 as in (A), and analyzed for osteolytic lesion formation after hematoxylin–eosin (H&E) staining. Representative H&E-stained images are shown on the left (scale bar, 100 μm). **D** Total RNAs were isolated from calvarial bones, and the expression levels of IRF8, MAFB, TMEM119 genes were quantified by RT-qPCR. Data represent the mean ± S.D. (n=6); ***p < 0.001 versus RANKL

Discussion

It has been known for years that VprBP triggers protein degradation through the proteasome pathway as a substrate-specific adaptor for E3 ubiquitin-ligase complex, but it is only recently that our studies have elucidated the

nuclear action of VprBP as a protein kinase [5–9]. Along with our demonstration of H2A and EZH2 as being phosphorylated by VprBP, our findings clearly established a new pathway in which VprBP inactivates growth regulatory genes and drives tumorigenesis [5–8]. Despite these

advances, however, little is known about other cellular processes that VprBP controls and the underlying mechanisms involved in its function. In the present study, we focused on a possible role for VprBP in regulating the differentiation process in which quiescent OCP cells are induced to become mature osteoclasts in response to RANKL stimulation. An initial finding from our investigation is that an increase in VprBP expression is closely related to elevated levels of H2AT120p in OCP-induced cells. These results raise the possibility that VprBP-mediated H2AT120p may contribute toward shutting off the genes encoding negative regulators of RANKL-induced osteoclastogenesis. Consistent with this idea, genome-wide transcriptome analysis demonstrated that genes targeted by VprBP in OCP-induced cells are heavily enriched in the network of genes whose expression is known to impair cell proliferation and differentiation. Since VprBP has no apparent effect on pro-osteoclastogenic genes, it seems to selectively antagonize the expression of anti-osteoclastogenic genes. Moreover, the fact that the presence of VprBP on target gene promoters is directly linked to enrichment of H2AT120p strengthens our claim that H2AT120p is a critical determinant of osteoclastogenic action of VprBP in OCP-induced cells. Adding further support to this idea, a selective inhibitor of VprBP, B32B3, is highly effective in blocking osteoclast differentiation *in vitro* as well as interfering with bone resorption and osteoporosis *in vivo*. This is the first study indicating that VprBP-mediated H2AT120p is a key histone mark in determining the rate of osteoclast differentiation and that controlling this epigenetic process might be a promising strategy for ameliorating osteoclast-related bone diseases.

We have previously shown that VprBP stimulates cancer cell growth through T367 phosphorylation (T367p) and stabilization of EZH2 and thereby H3K27me3-mediated gene silencing [8]. Although our initial study revealed a critical role for VprBP-mediated H2AT120p in osteoclast differentiation, whether the observed function of VprBP also requires its kinase activity targeting EZH2 was unclear. However, an intriguing observation we made in this regard is that EZH2 was expressed during the first two days of RANKL treatment while VprBP mRNA and protein levels increased mainly in the course of 3–5 days of RANKL stimulation. This observation is consistent with recent reports demonstrating the role of EZH2 at earlier time points of OCP cell differentiation [35, 36] and suggests that VprBP contributes to later stages of osteoclastogenesis mainly targeting H2AT120 as a substrate. Also, given that VprBP knockdown is ineffective at impairing EZH2 phosphorylation in RANKL-treated OCP cells, VprBP seems to rely more heavily on H2AT120p rather than EZH2T367p in driving osteoclast

differentiation. Such interpretation is further supported by our assays showing that VprBP target genes are not reactivated upon knockdown or inhibition of EZH2 in OCP-induced cells (not shown). Currently, we do not know the potential mechanism behind the selectivity of H2AT120p over EZH2 phosphorylation for VprBP function in OCP-induced cells, but our observation highlights the importance of H2AT120p in VprBP-driven anti-osteoclastogenic gene silencing and osteoclast differentiation. In the future, it will be interesting to determine how VprBP kinase activity is selectively targeted to H2A at certain stages of osteoclast differentiation, and how H2A phosphorylation process is functionally coupled with other epigenetic changes.

Another important question remaining to be answered is how VprBP-mediated phosphorylation of nucleosomal H2A affects the transcription of genes encoding anti-osteoclastogenic factors.

Recent studies demonstrated that H2AT120p can serve as a binding platform for the stable tethering and function of gene-regulatory factors at target genes in distinct chromatin regions [39, 40]. Considering such observations, it is reasonable to speculate that specific effector proteins are recruited to anti-osteoclastogenic genes by recognizing H2AT120p present on promoter nucleosomes. Mechanistically, this stable localization of effectors across the promoter regions of VprBP target genes establishes the inactive state of transcription, especially impeding transcription initiation, in OCP-induced cells. It is also possible that VprBP-mediated H2AT120p influences nucleosome structure by altering the interaction between H2A-H2B dimer and H3-H4 tetramer. H2A has a long carboxyl-terminal tail, and deletion of the tail domain increases the affinity of H2A-H2B dimer for the H3-H4 tetramer and inducing a conformational change in the nucleosome [41, 42]. The crystallographic structure of the nucleosome also indicates that the carboxyl-terminal domain of H2A is present in close proximity to the site where the DNA enters and exits the nucleosome [43]. Therefore, H2AT120p at its carboxyl-terminal tail is likely to generate a closing of the nucleosome at the DNA entry-exit points such that a compact nucleosome conformation is adopted to restrict the accessibility of nucleosomal DNA.

Keeping the balance between bone formation and resorption is tightly regulated by a number of transcriptional responses and coordinated signaling cascades in local microenvironments. Aberrant regulation of osteoclast formation and function has been implicated in bone loss with concomitant suppression of bone growth and repair. Since this misregulation can weaken the skeleton and increase the risk of fracture, targeting osteoclastogenic factors is a promising strategy to protect against

accelerated bone loss and preserve bone mass. The association of VprBP with bone disorders has not been reported so far. Therefore, our present study raises the possibility that VprBP could be a novel therapeutic target for osteoclastogenic disorders because of its critical role in OCP-induced cell differentiation into mature osteoclasts. In light of this view, VprBP-mediated inactivation of anti-osteoclastogenic genes described in this study will be very useful for the purpose of gaining further insight on the process to osteoclast formation and treating patients suffering from bone loss or skeletal complications of disease. Encouragingly, our studies have shown that VprBP inhibitor B32B3 not only blocks VprBP-induced osteoclastogenic gene silencing but can also reduce bone resorption and osteoporosis, both in vitro and in vivo. Osteoclastogenic signaling pathway is strictly controlled by a combination of gene specific transcription factors, which collectively maintain normal osteoclastic bone resorption within an acceptable level. In this respect, investigating how VprBP functionally cooperates with those multiple factors will also increase our understanding of osteoclastogenic function of VprBP as well as the molecular basis of disease associated with increased bone resorption.

Conclusions

Results presented here describe a role for VprBP-mediated H2AT120p in conferring inactive expression properties to anti-osteoclastogenic genes and enhancing the differentiation potential of OCP-induced cells. Importantly, treatment of OCP-induced cells with the VprBP inhibitor B32B3 potentiates anti-osteoclastogenic transcription program and impairs RANKL-induced osteoclast formation. These observations suggest that B32B3 could be used to regulate VprBP target genes and to treat bone resorption diseases such as osteoporosis and osteoarthritis.

Supplementary Information

The online version contains supplementary material available at <https://doi.org/10.1186/s13072-024-00561-7>.

Additional file 1.

Additional file 2.

Additional file 3.

Acknowledgements

Not applicable.

Author contributions

YS and WA conceived and designed the study. YS performed experiments with contributions of SK, TC, CK, WA, YS, and WA analyzed data. YS and WA wrote the manuscript. All authors read and approved the final manuscript.

Funding

The study was supported by the National Institutes of Health (AR073233). The study was also partly supported by award number P30CA014089 from the National Cancer Institute.

Data availability

The gene expression array data has been deposited in the NCBI Gene Expression Omnibus (GEO) database under the GEO accession number GSE275603.

Declarations

Ethics approval and consent to participate

Not applicable.

Competing interests

The authors declare no competing interests.

Received: 11 September 2024 Accepted: 18 November 2024

Published online: 26 November 2024

References

- Huang J, Chen J. VprBP targets Merlin to the Roc1-Cul4A-DDB1 E3 ligase complex for degradation. *Oncogene*. 2008;27:4056–64.
- Le Rouzic E, Belaidouni N, Estrabaud E, Morel M, Rain JC, Transy C, et al. HIV1 Vpr arrests the cell cycle by recruiting DCAF1/VprBP, a receptor of the Cul4-DDB1 ubiquitin ligase. *Cell Cycle*. 2007;6:182–8.
- McCall CM, Miliiani de Marval PL, Chastain PD, 2nd, Jackson SC, He YJ, Kotake Y, et al. Human immunodeficiency virus type 1 Vpr-binding protein VprBP, a WD40 protein associated with the DDB1-CUL4 E3 ubiquitin ligase, is essential for DNA replication and embryonic development. *Mol Cell Biol*. 2008; 28:5621–33.
- Zhang S, Feng Y, Narayan O, Zhao LJ. Cytoplasmic retention of HIV-1 regulatory protein Vpr by protein-protein interaction with a novel human cytoplasmic protein VprBP. *Gene*. 2001;263:131–40.
- Kim K, Kim JM, Kim JS, Choi J, Lee YS, Neamati N, et al. VprBP has intrinsic kinase activity targeting histone H2A and represses gene transcription. *Mol Cell*. 2013;52:459–67.
- Ghate NB, Kim S, Spiller E, Kim S, Shin Y, Rhie SK, et al. VprBP directs epigenetic gene silencing through histone H2A phosphorylation in colon cancer. *Mol Oncol*. 2021;15:2801–17.
- Shin Y, Kim S, Liang G, Ulmer TS, An W. VprBP/DCAF1 Triggers Melanoma-magentic Gene Silencing through Histone H2A Phosphorylation. *Biomedicines*. 2023; 11.
- Ghate NB, Kim S, Shin Y, Kim J, Doche M, Valena S, et al. Phosphorylation and stabilization of EZH2 by DCAF1/VprBP trigger aberrant gene silencing in colon cancer. *Nat Commun*. 2023;14:2140.
- Ghate NB, Kim S, Mehmood R, Shin Y, Kim K, An W. VprBP/DCAF1 regulates p53 function and stability through site-specific phosphorylation. *Oncogene*. 2023;42:1405–16.
- Matsuo K, Irie N. Osteoclast-osteoblast communication. *Arch Biochem Biophys*. 2008;473:201–9.
- Nakahama K. Cellular communications in bone homeostasis and repair. *Cell Mol Life Sci*. 2010;67:4001–9.
- Ash P, Loutit JF, Townsend KM. Osteoclasts derived from haematopoietic stem cells. *Nature*. 1980;283:669–70.
- Boyle WJ, Simonet WS, Lacey DL. Osteoclast differentiation and activation. *Nature*. 2003;423:337–42.
- Ikeda K, Takeshita S. Factors and mechanisms involved in the coupling from bone resorption to formation: how osteoclasts talk to osteoblasts. *J Bone Metab*. 2014;21:163–7.
- Raggatt LJ, Partridge NC. Cellular and molecular mechanisms of bone remodeling. *J Biol Chem*. 2010;285:25103–8.
- Teitelbaum SL. Bone resorption by osteoclasts. *Science*. 2000;289:1504–8.
- Baron R. Arming the osteoclast. *Nat Med*. 2004;10:458–60.
- Teitelbaum SL, Ross FP. Genetic regulation of osteoclast development and function. *Nat Rev Genet*. 2003;4:638–49.

19. Nakamura H, Nakashima T, Hayashi M, Izawa N, Yasui T, Aburatani H, et al. Global epigenomic analysis indicates protocadherin-7 activates osteoclastogenesis by promoting cell-cell fusion. *Biochem Biophys Res Commun*. 2014;455:305–11.
20. Li K, Han J, Wang Z. Histone modifications centric-regulation in osteogenic differentiation. *Cell Death Discov*. 2021;7:91.
21. Kim K, Punj V, Kim JM, Lee S, Ulmer TS, Lu W, et al. MMP-9 facilitates selective proteolysis of the histone H3 tail at genes necessary for proficient osteoclastogenesis. *Genes Dev*. 2016;30:208–19.
22. Kim K, Shin Y, Kim J, Ulmer TS, An W. H3K27me1 is essential for MMP-9-dependent H3N-terminal tail proteolysis during osteoclastogenesis. *Epigenetics Chromatin*. 2018;11:23.
23. Shin Y, Ghate NB, Moon B, Park K, Lu W, An W. DNMT and HDAC inhibitors modulate MMP-9-dependent H3 N-terminal tail proteolysis and osteoclastogenesis. *Epigenetics Chromatin*. 2019;12:25.
24. Shin Y, Kim S, Ghate NB, Rhie SK, An W. MMP-9 drives the melanomagenic transcription program through histone H3 tail proteolysis. *Oncogene*. 2022;41:560–70.
25. Shin Y, Kim S, Liang G, An W. MMP-9-dependent proteolysis of the histone H3 N-terminal tail: a critical epigenetic step in driving oncogenic transcription and colon tumorigenesis. *Mol Oncol*. 2024;18:2001–19.
26. Dobin A, Davis CA, Schlesinger F, Drenkow J, Zaleski C, Jha S, et al. STAR: ultrafast universal RNA-seq aligner. *Bioinformatics*. 2013;29:15–21.
27. Frankish A, Diekhans M, Ferreira AM, Johnson R, Jungreis I, Loveland J, et al. GENCODE reference annotation for the human and mouse genomes. *Nucleic Acids Res*. 2019;47:D766–73.
28. Zhao X, Valen E, Parker BJ, Sandelin A. Systematic clustering of transcription start site landscapes. *PLoS ONE*. 2011;6: e23409.
29. Du SJ, Frenkel V, Kindschi G, Zohar Y. Visualizing normal and defective bone development in zebrafish embryos using the fluorescent chromophore calcein. *Dev Biol*. 2001;238:239–46.
30. Bergen DJM, Kague E, Hammond CL. Zebrafish as an emerging model for osteoporosis: a primary testing platform for screening new osteoporosis compounds. *Front Endocrinol (Lausanne)*. 2019;10:6.
31. Dietrich K, Fiedler IA, Kurzyukova A, Lopez-Delgado AC, McGowan LM, Geurtzen K, et al. Skeletal biology and disease modeling in zebrafish. *J Bone Miner Res*. 2021;36:436–58.
32. Chen JR, Lai YH, Tsai JJ, Hsiao CD. Live Fluorescent Staining Platform for Drug-Screening and Mechanism-Analysis in Zebrafish for Bone Mineralization. *Molecules*. 2017;22.
33. Kim J, Shin Y, Lee S, Kim M, Punj V, Lu JF, et al. Regulation of Breast Cancer-Induced Osteoclastogenesis by MacroH2A1.2 Involving EZH2-Mediated H3K27me3. *Cell Rep*. 2018; 24:224–37.
34. Kim JM, Shin Y, Lee S, Kim MY, Punj V, Shin HI, et al. MacroH2A1.2 inhibits prostate cancer-induced osteoclastogenesis through cooperation with HP1alpha and H1.2. *Oncogene*. 2018; 37:5749–65.
35. Adamik J, Pulugulla SH, Zhang P, Sun Q, Lontos K, Macar DA, et al. EZH2 Supports osteoclast differentiation and bone resorption via epigenetic and cytoplasmic targets. *J Bone Miner Res*. 2020;35:181–95.
36. Chen J-R, Lazarenko O, Gai D, Li C, Blackburn M, Zhan F. Ezh2 mediates epigenetic regulation of osteoclastogenesis and bone remodeling in mice. *bioRxiv*; 2021.
37. Barrett R, Chappell C, Quick M, Fleming A. A rapid, high content, in vivo model of glucocorticoid-induced osteoporosis. *Biotechnol J*. 2006;1:651–5.
38. He H, Wang C, Tang Q, Yang F, Xu Y. Possible mechanisms of prednisolone-induced osteoporosis in zebrafish larva. *Biomed Pharmacother*. 2018;101:981–7.
39. Liu H, Qu Q, Warrington R, Rice A, Cheng N, Yu H. Mitotic transcription installs Sgo1 at centromeres to coordinate chromosome segregation. *Mol Cell*. 2015;59:426–36.
40. Zhang M, Liang C, Chen Q, Yan H, Xu J, Zhao H, et al. Histone H2A phosphorylation recruits topoisomerase IIalpha to centromeres to safeguard genomic stability. *EMBO J*. 2020;39: e101863.
41. Vogler C, Huber C, Waldmann T, Ettig R, Braun L, Izzo A, et al. Histone H2A C-terminus regulates chromatin dynamics, remodeling, and histone H1 binding. *PLoS Genet*. 2010;6: e1001234.
42. Bendandi A, Patelli AS, Diaspro A, Rocchia W. The role of histone tails in nucleosome stability: an electrostatic perspective. *Comput Struct Biotechnol J*. 2020;18:2799–809.
43. Luger K, Mader AW, Richmond RK, Sargent DF, Richmond TJ. Crystal structure of the nucleosome core particle at 2.8 Å resolution. *Nature*. 1997; 389:251–60.
44. Luger K, Rechsteiner TJ, Flaus AJ, Wayne MM, Richmond TJ. Characterization of nucleosome core particles containing histone proteins made in bacteria. *J Mol Biol*. 1997;272:301–11.
45. Shukla MS, Syed SH, Goutte-Gattat D, Richard JL, Montel F, Hamiche A, et al. The docking domain of histone H2A is required for H1 binding and RSC-mediated nucleosome remodeling. *Nucleic Acids Res*. 2011;39:2559–70.

Publisher's Note

Springer Nature remains neutral with regard to jurisdictional claims in published maps and institutional affiliations.